A spherical harmonics-based framework for representing steady-state shifts in neuron models induced by weak electric fields

Adrià Galan-Gadea[1], Ricardo Salvador[1], Fabrice Bartolomei[2], Fabrice Wendling[3] and Giulio Ruffini[1]‡

[1] Neuroelectrics, Av. Tibidabo 47b, 08035 Barcelona, Spain

[2] Clinical Physiology Department, INSERM, UMR 1106 and Timone University Hospital, Aix-Marseille Université, Marseille, France

[3] Univ Rennes, INSERM, LTSI (Laboratoire de Traitement du Signal et de l'Image) U1099, 35000 Rennes, France

E-mail: `giulio.ruffini@neuroelectrics.com`

Abstract. *Objective:* We provide a systematic framework for the quantification of the effect of externally applied weak electric fields on realistic neuron compartment models as captured by physiologically relevant quantities such as the membrane potential or transmembrane current as a function of the orientation of the field. *Approach:* We define a response function as the steady-state change of the membrane potential induced by a canonical external field of 1 V/m as a function of its orientation. We estimate the function values through simulations employing reconstructions of the rat somatosensory cortex from the Blue Brain Project. The response of different cell types is simulated using the NEURON simulation environment. We represent and analyze the angular response as an expansion in spherical harmonics. *Main results:* We report membrane perturbation values comparable to those in the literature, extend them to different cell types, and provide their profiles as spherical harmonic coefficients. We show that in resting condition, responses are dominated by their dipole terms ($\ell = 1$), in agreement with experimental findings and compartment theory. Indeed, we show analytically that for a passive cell only the dipole term is nonzero. However, for states other than resting, other terms, while small, appear relevant. In particular, we show how $\ell = 0$ and $\ell = 2$ terms can modify the function to induce asymmetries in the response. *Significance:* This work provides a practical framework for the realistic representation of the effects of weak electric fields on different neuron types and their main regions—an important milestone for the development of micro- and mesoscale models and the optimization of brain stimulation solutions.

Keywords: tDCS, weak electric fields, non-invasive brain stimulation, compartment models

Submitted to: *J. Neural Eng.*

‡ giulio.ruffini(at)neuroelectrics.com

1. Introduction

Transcranial electrical stimulation (tES) is a non-invasive neuromodulatory technique based on accurate control of weak currents injected in the scalp from multiple channels and of the resulting electric fields induced in the brain. tES, pioneered by Nitsche and Paulus [1], includes both direct and alternating current variants known as tDCS and tACS. Low intensity, controlled currents (typically $\sim$1 mA but $<$4 mA) are applied through scalp electrodes in repeated 20–60 min sessions. The subtle but persistent modulation of neuronal activity is believed to lead to plastic effects deriving from Hebbian mechanisms.

The current evolution of this and related techniques such as transcranial magnetic stimulation, elecroconvulsive therapy or deep brain stimulation is veering towards model-driven approaches and optimization principles based on a mechanistic understanding of pathophysiology, the interaction of the electric field with neuron populations and the resulting dynamical, and then plastic, effects [2, 3]. In this work we aim to quantify in a systematic way the response of different cell types and cell parts to be used in future approaches of model-driven stimulation.

The concurrent effects of tES currents on the brain are thought to be mediated by the interaction of the generated electric field with cortical neurons [4, 5]. These electric fields are weak ($\sim$1 V/m) [6], relatively large-scale (with spatial correlation scales of the order of a few cm) and induce small changes in the membrane potential of cells (sub-mV) [7, 8]. Polarization happens in a compartment-specific manner [9, 10, 11], hyperpolarizing compartments close to the virtual anode and depolarizing those close to the virtual cathode. Furthermore, from cable theory it is expected that changes in the electric field along neuron fibers cause local depolarizations as well. Then, the effect in a cell under the same stimulation can have very different responses locally. Particularly, where fibers bend and mostly where terminations, effects are significantly larger [12]. Thus, the overall morphology is key to explain effects observed locally. To take all effects into account, we use multi-compartment models that allow both to locally couple the field to realistic morphology models and to make predictions of the induced perturbations [13].

Pyramidal cells have been of particular interest in the field for two reasons. First, they are elongated, which leads to the generation of a larger membrane perturbation when field and neuron are aligned [8]. Secondly, they are spatially organized. Because of this and because of the spatial homogeneity of the electric fields, the effects on such cells are spatially coherent and thought to lead to stronger, network enhanced effects [14, 15]. In contrast, effects on interneurons are usually disregarded due to their small size and non-elongated branching profiles [8].

So-called hybrid models combining physics and physiology represented by computational models of brain networks can be used to represent pathophysiology and the effects of electric fields [16, 17]. A widely used example of physiology models at the mesoscale are neural mass models [18, 19, 20] (NMM) and their more recent

extensions (NMM2) [21, 22, 23]. To be used in model-driven stimulation, they all require a description of the electric field in the cortex — which can be provided using realistic finite element modeling [5, 24] — as well as an interaction model for the effects of the field on neuron populations. In the case of classical neural mass models (NMM), this can be provided from an estimation of the field-induced changes in membrane potential or transmembrane current in relevant compartments such as the soma at population level. A useful staring point to for this is modeling the effects at the single cell level.

In this paper we focus on characterizing the effects of the weak electric field on the stable equilibrium of single neuron models using expansions in terms of spherical harmonics. With this approach we aim to provide (i) a systematized version of describing the angular dependence of the response through simulations, (ii) a framework that allows averaging to describe cell parts and types, (iii) a representation in meaningful terms that represent the dipolar behaviour on its own but accounts for other angular dependence profiles if necessary. We validate the common dipolar approach and show that it is accurate for small perturbations induced at neurons at rest (far from threshold) and show that is exact for the passive membrane. Nevertheless, we observe that corrections to pure dipolar responses may need to be applied closer to threshold in realistic neurons.

2. Methods

2.1. Formalism for steady-state changes induced by an electric field

We will be studying here the response of a neuron to a constant, uniform weak electric field. The field is characterized by a magnitude $E \equiv ||\mathbf{E}||$ and an orientation that can be expressed with two spherical angles, the polar angle θ and the azimuth φ. Thus, in spherical coordinates the electric field is given by

$$\mathbf{E} = E\,(\sin\theta\cos\varphi\,\mathbf{e}_x + \sin\theta\,\sin\varphi\,\mathbf{e}_y + \cos\theta\,\mathbf{e}_z) \equiv E\,\hat{\mathbf{e}} \tag{1}$$

Let us consider a variable v that characterizes a physiologically relevant magnitude that is affected by an external electric field. In our study, we focus on the membrane potential but the formalism can be extended to other variables, e.g., transmembrane currents. If the variable v has a stable equilibrium, i.e., resting potential in our case, we expect that the applied electric field will shift that equilibrium to a new value of v. We aim to quantify that induced change δv of the steady-state solution for different realistic models of cell types. In our case, this shift is commonly referred to as polarization. Assuming that the polarization δv scales linearly with E [8], we can include the dependency of the shift with the orientation of the field with a function defined on a sphere $\Phi(\theta, \varphi)$ i.e. that has a value for any direction in space. We refer to Φ as the *response function*, which is a function valued the shift δv under an electric field of 1 V/m in a given direction. Under these assumptions§, δv can be expressed as shown in Equation 2.

$$\delta v = E\,\Phi(\hat{\mathbf{e}}) = E\,\Phi(\theta, \phi) \tag{2}$$

2.2. Expansion in spherical harmonics

Spherical harmonics form a complete and orthonormal set of functions $Y_{\ell m}$ defined on the surface of the sphere (parametrized by two spherical angles, θ and φ), where ℓ and m refer to the degree and the order of the harmonic respectively. Squared-integrable functions defined on the sphere can be expressed as a sum of spherical harmonic terms much as functions on the plane can be expressed as a Fourier series. In fact, both spherical harmonics and complex exponential are eigenfunctions of equations associated to the Laplace partial differential equation in different manifolds (the plane and the sphere). As the response function $\Phi(\theta, \varphi)$ is a function on the sphere, it can be expanded in terms of spherical harmonics, meaning that it can be expressed as in Equation 3 and fully characterized by a set of coefficients $f_{\ell m}$,

$$\Phi(\theta, \varphi) = \sum_{\ell=0}^{\infty} \sum_{m=-\ell}^{\ell} f_{\ell m} Y_{\ell m}(\theta, \varphi) \tag{3}$$

§ More generally, we can start from $\delta v(\mathbf{E}) = \delta v(E, \hat{\mathbf{e}}) = \Phi_0(\hat{\mathbf{e}}) + E\Phi_1(\hat{\mathbf{e}}) + \frac{1}{2}E^2\Phi_2(\hat{\mathbf{e}}) + ...$ The first term is zero here by definition.

Spherical harmonics are characterized by a degree and order pair (ℓ, m), see Appendix A for a definition. They are tightly linked to the multipole expansion, so one can think of the $\ell = 0$ term as a *monopole* behaviour, which is a term that does not depend on orientation. The $\ell = 1$ terms represent a dipolar behaviour, $\ell = 2$ a quadropole, and so on. Finally, under a parity transformation, where a point with coordinates $\{\theta, \phi\}$ changes to $\{\pi-\theta, \pi+\phi\}$ (corresponding to a reversal of the orientation of the electric field in our case),

$$Y_{\ell m}(\theta, \varphi) \to Y_{\ell m}(\pi - \theta, \pi + \varphi) = (-1)^{\ell} Y_{\ell m}(\theta, \varphi) \tag{4}$$

This means that if we expect the membrane response to change sign under electric field reversal (e.g., if it is linear in $\mathbf{E}$), only odd ℓ terms should contribute to the expansion.

2.2.1. The λE linear model is contained in the $\ell = 1$ terms of the expansion The f_{1m} terms can be seen to correspond to the λE (dipole) model, where the induced polarization is represented as the dot product of the electric field vector $\mathbf{E}$ and a vector $\boldsymbol{\lambda}$ of magnitude the length constant of the membrane and in the orthodromic direction of the cell. We can rewrite the λE model as

$$\delta v = \boldsymbol{\lambda} \cdot \boldsymbol{E} = E\, \boldsymbol{\lambda} \cdot \boldsymbol{e} = E\, (\lambda_x \sin\theta \cos\varphi + \lambda_y \sin\theta \sin\varphi + \lambda_z \cos\theta) \tag{5}$$

which is seen to correspond to the $\ell \neq 1$ terms in the expansion, with λ_z is represented by f_{10}, λ_x by f_{11} and λ_y by f_{1-1}. The λE model translates to symmetric depolarization under anodal stimulation and hyperpolarization under cathodal stimulation.

2.3. Cell models

We use the multi-compartment conductance-based models from the cortical microcircuit reconstruction by the Blue Brain Project [25]. Model morphologies are based on reconstructions from real acquisitions from juvenile rats. In this work we consider all the morphology types in the database except the layer I interneurons. That includes 9 types of interneurons: bipolar, bitufted, chandelier, double bouquet, Martinotti, neurogliaform and basket cells (including large, small and nest). These 9 types make 36 morphology types, one of each for each layer (II/III, IV, V and VI). Regarding excitatory cells, there are 13 morphology types (12 types of pyramidal cells and spiny stellate cells). All morphologies are made of connected cables, as required by the NEURON simulation environment (v8.0.0). Each cable is discretized in evenly spaced compartments. All cables were assigned a minimum of one compartment and were added two compartments every 40 µm of length. The biophysical membrane models contain 13 different known Hodgkin-Huxley type ion channel models distributed using different criteria along the morphology. In the original work, the Blue Brain Project team defined 11 types of ion channel profiles or *electrical types* in a way that exhibit different spiking features. The options unfold into 10 inhibitory and 1 excitatory electric profiles, where the latter is the one representing all excitatory cell models of the dataset

(continuous adapting, cAD). Regarding inhibitory cells, they included bursting (b), continuous (c) and delayed (d) models, later subdivided into accomodating (AC), non-accomodating (NAC), stuttering (STUT) and irregular (IR). Irregular spiking models contain stochastic potassium channels that introduce stochasticity into their behaviour. For this study we supressed these because of the incompatibility with our framework. Moreover, we discarded electric types generating spontaneous spiking at rest: cNAC, cSTUT and dNAC. Given that the same morphology types were found to show different electrical types, they created models for each morphoelectrical combination. Then, the models dataset has 5 statistical clones of each morphoelectrical type.

2.3.1. Uniform electric field coupling The coupling of the external electric field to the neuron models is implemented via the extracellular potential in NEURON 8.0.0. To access the extracellular potential at each compartment we use the `extracellular` mechanism, and to attach the value induced by the external electric field we tweak the `xtra` mechanism for extracellular recording and stimulation, based on the approach by McIntyre and Grill [26]. Recall that the extracellular potential is related to the external uniform field by $\mathbf{E} = -\boldsymbol{\nabla} V_{\text{ext}}$, with

$$V_{\text{ext}}(x, y, z) = -E\big(x \sin\theta \cos\varphi + y \sin\theta \sin\varphi + z \cos\theta\big) \tag{6}$$

Here (x, y, z) refers to the spatial coordinates in $\mathbb{R}^3$ of the center of a compartment of the neuron model.

2.4. Spherical harmonics-based representation

Following the expansion introduced in Equation 2, once $\hat{\Phi}(\theta, \varphi)$ has been estimated for each compartment, it is represented by a set of spherical harmonics coefficients. The calculation is performed with the `pyshtools` Python package, using a 4π-normalization and the Condon-Shortley phase factor convention [27]. The coefficients $f_{\ell m}$ fully represent the response function $\Phi(\theta, \varphi)$ and they can be assessed integrating the response function over the sphere. Using the 4π normalization, it reads as a double integral

$$f_{\ell m} = \frac{1}{4\pi} \int_0^{2\pi} d\varphi \int_0^{\pi} d\theta \sin\theta \, \hat{\Phi}(\theta, \varphi) Y_{\ell m}(\theta, \varphi) \tag{7}$$

2.5. Response function estimation

Let $\hat{\Phi}(\theta, \varphi)$ be the discretized estimation of the response function. $\hat{\Phi}(\theta, \varphi)$ can be defined as a collection of changes δv observed for different orientations, where the particular orientations set is determined by the sampling method and the chosen resolution. We obtain $\hat{\Phi}(\theta, \varphi)$ performing simulations applying electric fields of 1 V/m of magnitude in different orientations to a resting neuron model using the NEURON simulation environment (v8.0.0) [28]. All experiments are performed at temperatures of $T = 36.9°\text{C}$ to mimic normal physiological temperatures of living human brains [29].

2.5.1. Temporal design of the simulation experiment The simulation pipeline to estimate the steady-state response of any neuron model under an electric field consists of two phases: (1) computing the resting state, and (2) applying an electric field to estimate the change in the induced change in the steady-state condition. The resting state is defined as the steady-state solution of the system when no external stimulation is present. It is assessed by letting the system converge until it experiences no further change in its state variables. Computationally this requirement is defined to be met when the membrane potential varies less than 1 nV anywhere in the cell without further external inputs. The second phase consists in assessing the displacement of the steady-state solution under an external perturbation, see Figure 1.D. The system is initialized in the pre-computed resting state. Then, the shift in the steady-state solution is retrieved as the change experienced after 500 ms of 1 V/m uniform electric field application in a given condition. The induced change, i.e., δv, is computed with respect to the control condition with no field applied. All simulations are integrated using the fully implicit backward Euler method with an integration time step of 25 µs.

2.5.2. Experimental conditions To characterize the response function, we assess the induced changes for a different set of orientations. We use the Type I Driscoll-Healy sampling of the sphere (DH1), using N=12 to reconstruct harmonics until a maximum degree of $\ell_{\max} = 5$. The relationship among both is given by the sampling theorem: $\ell_{\max} = N/2 - 1 = 5$. The DH1 sampling consists on sampling both θ and φ in N points each, building an $N \times N$ grid covering the sphere [30]. Because the full span of both angular dimensions is used, the polar resolution ($\Delta\theta$) is half of the azimuthal one ($\Delta\varphi$). For $N = 12$, the angular distance among consecutive sampled points is of $\Delta\varphi = 2\pi/13$ and $\Delta\theta = \pi/13$ rad. The discretization is shown in Figure 1.B.

2.6. Averaging response functions

A response function can be derived for each compartment of a cell model through the methodology already described above, v. Figure 1. However, in the context of model-driven stimulation, the interest lies in having simplifications of the complex morphology. Due to linearity, *lumped* response functions can be obtained by averaging the coefficients. We exploit this to create two types of models: response functions of (i) cell parts and (ii) cell types. The multi-compartment models here used have hundreds of compartments for each cell along their morphology. Each compartment can be tagged to belong to a specific region or part of the cell. We use the models original classification of axon, soma and dendrites, with a further distinction of apical and basal dendrites in the case of pyramidal cells. In the case of apical dendrites, we make a further distinction between those found in LI with respect to the rest. To build models of cell types, we use the different clones available in the database belonging to a same cell type. We averaged the models of the different cell parts of the clones of the same type and this way built a canonical model for that type.

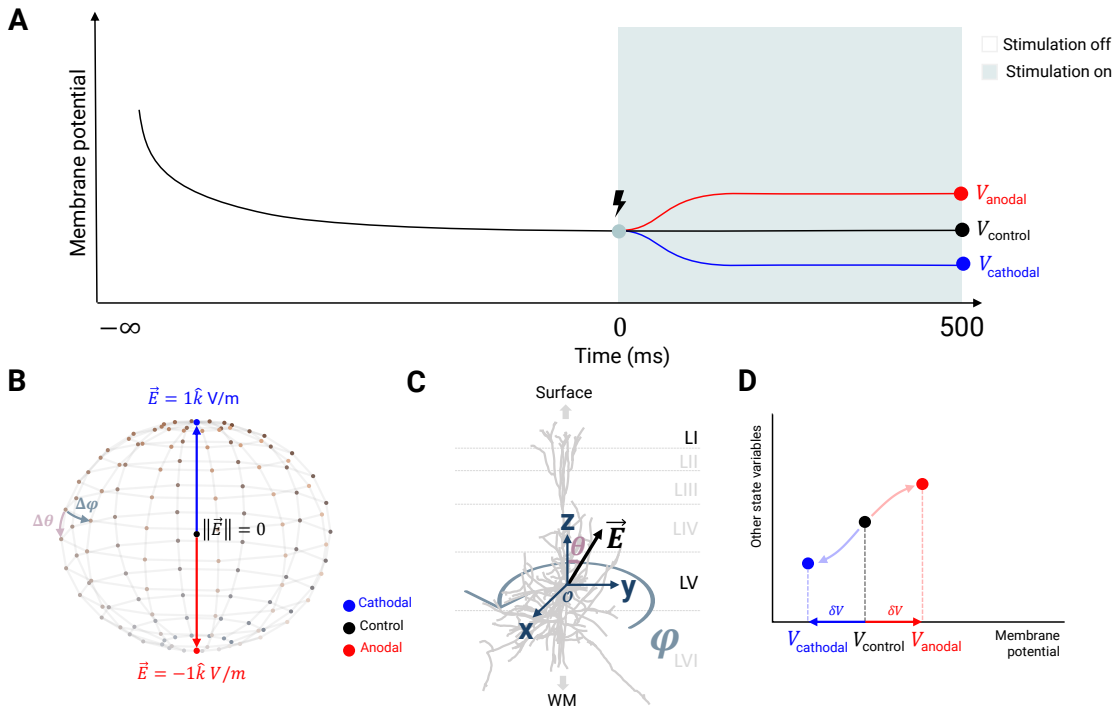

Figure 1. Experimental design for estimatation of the response function. A. Temporal profile of the simulation of different experimental conditions. The first part of the experiment computes the resting condition of the model and is common for all experimental conditions. The latter consists in applying a constant external electric field and is repeated of all the desired orientations of the electric field. **B. Experimental conditions.** Anodal (red), cathodal (blue) and control (black) conditions in the context of the DH1 Sampling of the sphere. The grid represents the $N \times N$ sampling of the sphere with $N = 12$, with points separated by $\Delta\theta = \pi/13$ and $\Delta\varphi = 2\pi/13$ [30]. **C. Coordinate system** definition with respect to the cell. The vertical direction represents the component normal to the cortical surface and corresponds to the z Cartesian coordinate. The spherical coordinates represent with θ the inclination and with φ the azimuth. The radius is the magnitude of the field E. For all cell models, the origin of coordinates O is set at the center of the soma. **D. Stimulation as an attractor shift.** A constant applied field changes the steady-state condition. In the soma of a prototypical pyramidal cell, the state is shifted towards a depolarized membrane potential.

2.7. Realistic montage

Based on the λE approach, one logical strategy is to optimize for the normal component of the electric field with respect to the cortical surface. The quantification of the performance of the montage is carried out by averaging the electric field on the target area. Expressions like the λE model, which captures the main response of neurons to the fields can be used to develop metrics that are more representative of the relevant physiological effects of the stimulation. As an example of this, we performed a montage optimization to stimulate the dorsolateral prefrontal cortex, which is a common area

for stimulation in tDCS, in a real head model (figure 9.A). We ran the Stimweaver algorithm [24] with a maximum of 8 channels and a total injected current of 4.0 mA, under the restriction of 2.0 mA maximum per channel. The montage was optimized to achieve an normal component to the cortical surface of the electric field of 0.25 V/m within the target, using weights of 10 and 2 to on- and off-target nodes respectively. We computed the predicted average membrane polarization of LV pyramidal cells somata on- and off-target as a proof of concept (Figure 9).

3. Results

3.1. The response function at rest is dipolar

Consistent with the analysis of the passive cell (see Appendix B), the response function is dipolar under weak fields at rest. During stimulation, each cell compartment reaches a new steady-state solution. The maximum observed somatic polarization corresponds to fields parallel to the somato-dendritic axis and at 0.14 mV per 1 V/m in layer V early-branching thick-tufted pyramidal cells. These values are in line with the literature as with results reported in CA1 pyramidal cells [31] and comparable to the typically assumed value of 0.2 mV per V/m of applied electric field [8].

3.2. Somatic polarizations in excitatory cells

Consistent with previous findings, the most affected cells are pyramidals of subgranular layers (V and VI), with an increased effect on those with an apical tuft. The largest effect is observed in the early-branching thick tufted population, due to the asymmetry of the processes distribution with respect to the soma. The variety of layer VI pyramidal cells is accompanied by different responses as well. Somatic polarization in the LVI tufted cell models is at 0.10 mV, i.e., 58% larger than in the untufted, at 0.07 mV. Somata of inverted pyramidals show an effect of size comparable to that of tufted cells i.e. 0.10 mV but with reversed polarity. In supragranular layers, effects on pyramidal cells were found to be very small and irrelevant on spiny stellate and star pyramidals. All maximum somatic polarizations found in the different averaged pyramidal cell models are compiled in Table 1.

3.3. Somatic polarizations in interneurons

Due to its central position with respect to other cell processes, effects in the soma of interneurons are rather small compared to pyramidal cells. Restricting the electrical type to continuous accomodating (cAC) models, we observe a large variety of responses across morphologies and layers—see Figure 4. In bipolar, bitufted, chandelier and double bouquet cells we observe a reversal of the polarity of the effect at the soma between supragranular and infragranular layers. Martinotti cell models show the lowest variability between layers. Basket cells are the group that display the smallest response at the level of the soma consistently in their different types (large, nest and small) and layers. On the other hand, the cell type model displaying the largest somatic effect are bipolar cells. In this particular cell morphology, the size of the effect strongly depends on its electrical type (see Figure 5). However, we do not observe such a dependence in the other types of interneurons.

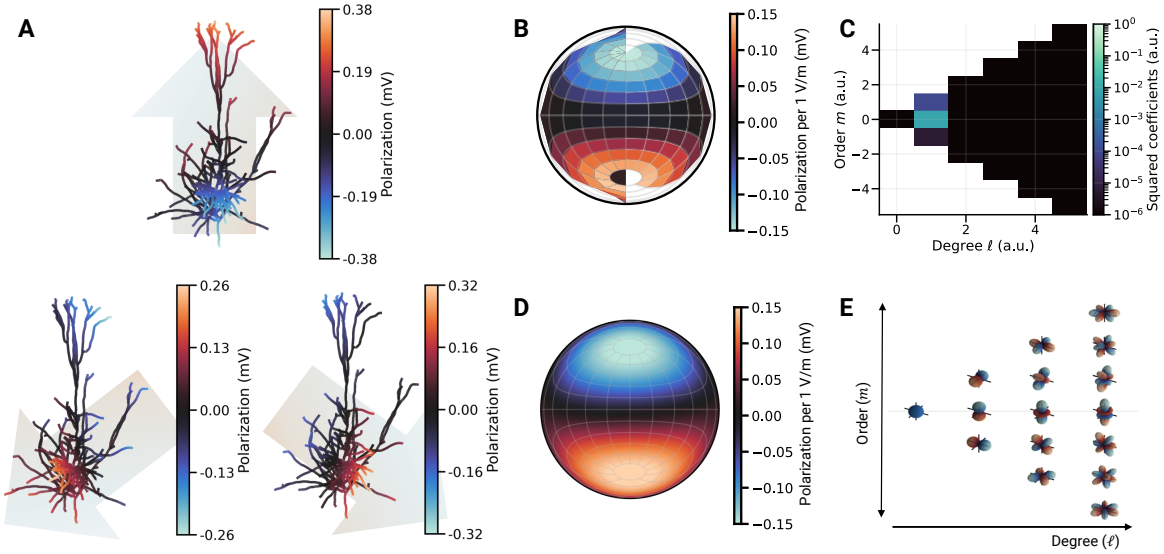

Figure 2. Polarization dependence on the electric field orientation. A. Polarization of the membrane under a uniform electric field of 1 V/m. The direction of the external electric field has a direct impact on how the charges are redistributed along the cell morphology. In this example, the effects on a layer V pyramidal cell model are displayed for an applied external electric field of 1 V/m in the direction of the background arrows displayed below each cell. **B. Somatic response function estimate.** Estimated polarization of the soma under a 1 V/m electric field for each orientation of the DH1 sampling as described in Figure 1.B. The 2D projection is used with the Lambert method, where the azimuthal angle matches the horizontal axis. **C. Spherical harmonics spectrum.** Representation of each spherical harmonic coefficient squared. Only the $\ell = 1$ terms are present, i.e., the response is dipolar. The description in spherical harmonics terms displays a strong predominance of the $(\ell = 1, m = 0)$ indicating an alignment with the z-axis (see Figure 1.C) slightly tilted towards the x-axis as determined by the presence of a small $(\ell = 1, m = 1)$ term. **D. Reconstructed response function.** Continuous version of the response function represented by the coefficients. It represents all the information contained in the sampled estimate shown in B. **E. Spherical harmonics.** Polar representation of all spherical harmonics up to $\ell = 3$ in the same layout as in C for an intuitive interpretation of each of the coefficients. The magnitude of the function for each orientation sizes the radius and the color codes the sign, warm and cold being positive and negative respectively.

3.4. Effects on different cell parts can be represented with different response functions

As expected from the pre-existing literature on the field, different parts of pyramidal cells respond differently to the presence of the field. The estimated response functions for the different cell parts, obtained through averaging the responses of the individual compartments belonging to each region, display the classical response of the apical dendrites with a reversed polarity compared to the one observed in the soma and the

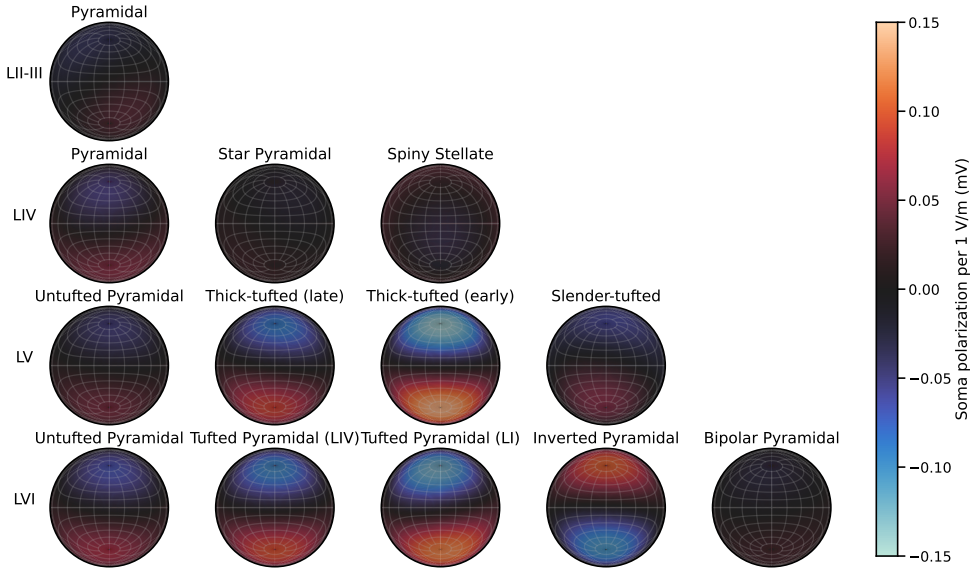

Figure 3. Polarization of soma of pyramidal cells under 1 V/m electric field. Each row represents a neocortical layer and each column a pyramidal cell type. Each plot displays the modeled change of the membrane potential (mV) in the soma due to an external electric field of 1 V/m as a function of the relative orientation of the electric field. Orientation dependence is represented using a Lambert projection. The vertical axis codes the polar angle θ which ranges from $\theta = 0$ in the top (indicating a vertically aligned electric field pointing up) to $\theta = \pi$ (down) in the bottom. The horizontal axis is the azimuthal angle φ, where the left end is $\varphi = 0$ and the right one is $\varphi = 2\pi$. "*Early*" and "*late*" in layer V (LV) thick-tufted pyramidal cells refer to when the apical dendrites branching of the tuft begins. In LVI tufted pyramidal cells, the layer in parenthesis is the layer in which the dendritic tuft terminates.

basal dendrites, e.g., hyperpolarized under anodal stimulation, see Figure 6. The largest response among the explored regions is found in the apical dendrites contained in layer I. In the example of the figure, the polarization in the direction where effect is maximum reaches 0.24 mV per V/m in layer I apical dendrites, whereas it is only of 0.03 mV at the trunk, defined as the compartments from the apical tree found from layer II down. When averaging the whole of the apical dendritic tree, the response function is reduced to a maximum of 0.07 mV (per V/m). The soma and the basal dendrites display a similar pattern, with a maximum polarization of 0.16 in the soma and of 0.18 mV in the basal dendrites. In the axon, including the descendant and the collaterals, the average is smaller at 0.04 mV per V/m.

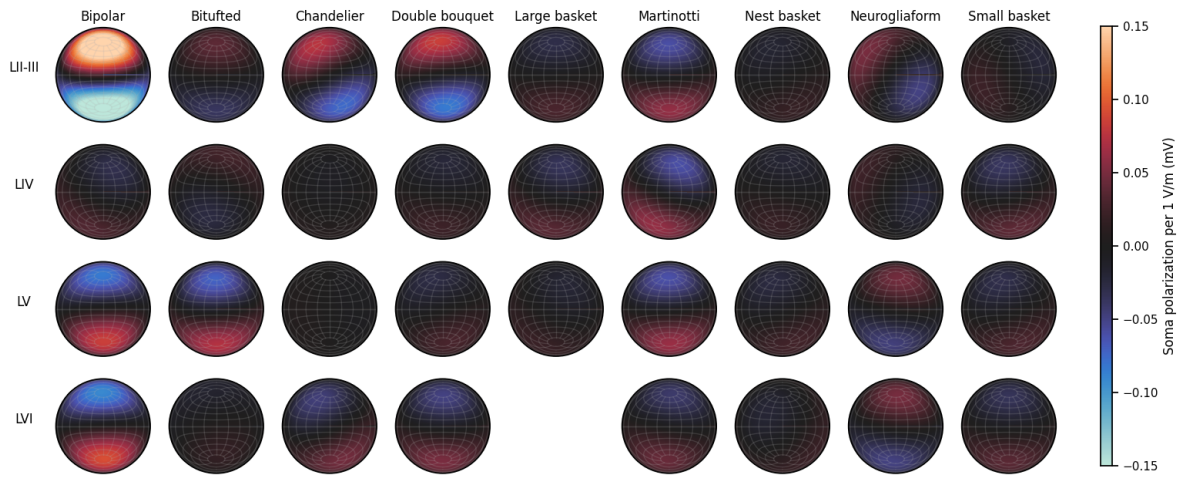

Figure 4. Polarization of soma of interneurons under 1 V/m electric field. Simulations of the average membrane potential change (mV) in the soma in continuous accomodating (cAC) models of interneurons. Rows and columns represent cortical layers and morphology types respectively. The color range is set to match that of Figure 3 to ease comparison with pyramidal cells. Bipolar cell models of layers II-III appear saturated because their polarization values exceed the 0.15 mV. Large basket cell models for LVI are not available in the original set of models.

3.5. The direction and magnitude of the effect depend on the cell state

We observe that injecting hyperpolarizing and depolarizing currents in the soma of the layer V pyramidal cell model (prior to the application of the E-field), the response function changes. It keeps displaying a dipolar behavior for most values, purely captured by the $\ell = 1$ coefficients. Moreover, the most relevant term in all the states is the dipole in the direction parallel to the normal to the cortical surface, i.e., aligned with the z-axis ($\ell = 1, m = 0$) as in Figure 1.C. Under a hyperpolarizing current, we observe a small increase of the effect saturating at 0.17 mV per V/m. Under depolarizing currents, we observe two different types of behaviour. For currents up to 0.25 nA (corresponding to a membrane potential of ∼-62.50 mV, 10 mV above resting) we observe a decrease in the magnitude of the effect reaching a minimum at 0.12 mV per V/m in the direction of maximum effect. We observe a different behavior for currents above 0.2 nA until the system enters a spiking regime for currents above 0.34 nA, corresponding to potentials over -58.13 mV. In this window we observe a rapidly increasing effect and the emergence of a non-dipolar response. The response becomes asymmetric, i.e., the magnitude of the effect of anodal and cathodal stimulations of equal field magnitude is not the same. Still, fields perpendicular to the axis of the *dipole* have negligible effects. In spherical harmonics terms this is observed as the emergence of a pair of $\ell = 0$ and $\ell = 2$ terms that increases with the size of the asymmetry, being largest at the verge of the bifurcation. Right before the bifurcation we report an effect of anodal stimulation of

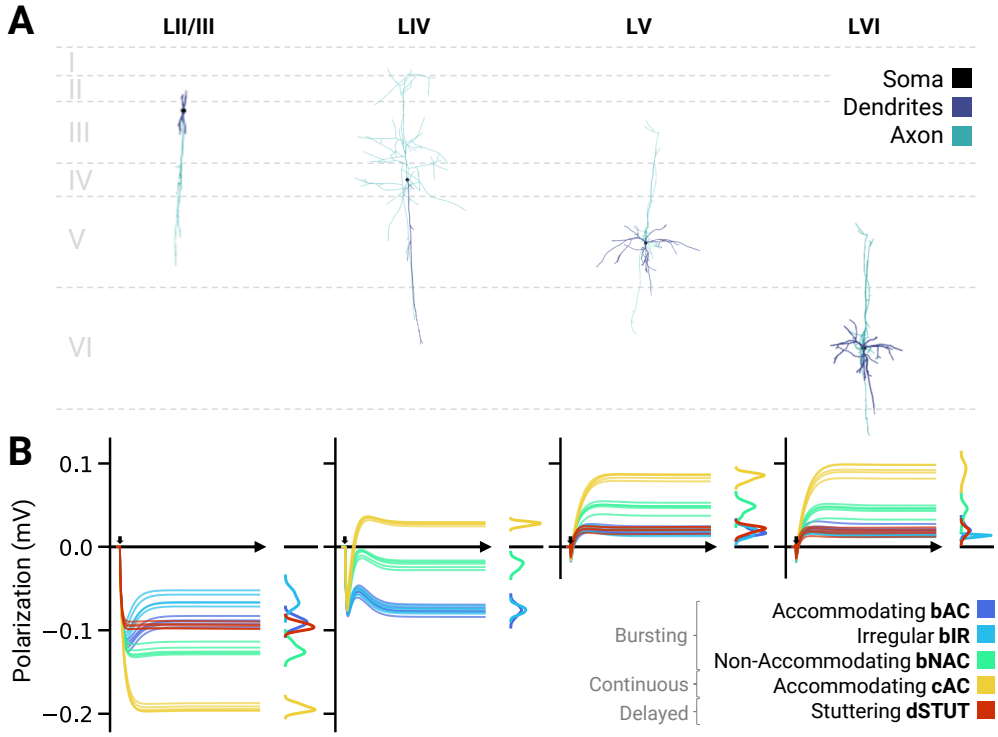

Figure 5. Effect differs across electrical types of bipolar cells. A. Morphology examples of bipolar cells of different layers. **B.** Somatic responses of the different cell models under anodal stimulation of 1 V/m. Each plot provides the polarization curves as a function of time of the models of bipolar cells of a given layer. The stimulation onset is marked as a small arrow over the horizontal axis. The total stimulation duration is of 500 ms. At the right of each plot, the plot is extended with the distribution of the end-polarization states.

0.35 mV, whereas cathodal stimulation shifts the membrane potential by -0.26 mV. The asymmetry is thus of 0.61 mV at that point.

3.6. Summary response functions can be used in a realistic montage

We optimized a montage using the stimweaver algorithm [24] to induce a 0.25 V/m field normal to the cortical surface pointing inwards in the dlPFC, i.e., on-target (Figure 9.A). The optimized montage is shown in Figure 9.B together with the predicted electric fields on the cortex—overlaid on the brain morphology. The normal component on-target predicted with the optimized montage has a median value across nodes of 0.11 V/m, and a mode of 0.17 V/m computed as the maximum of the kernel density estimate. Through the formalism in Equation 2 and the computationally derived response functions, that map can be translated to a variable with actual physiological meaning, e.g., the somatic membrane potential perturbation of LV early branching thick-tufted pyramidal cells, Figure 9.C. We observe a significant effect on-target (Mann-Whitney U, $p < 1 \times 10^{-3}$, see Figure 9.D).

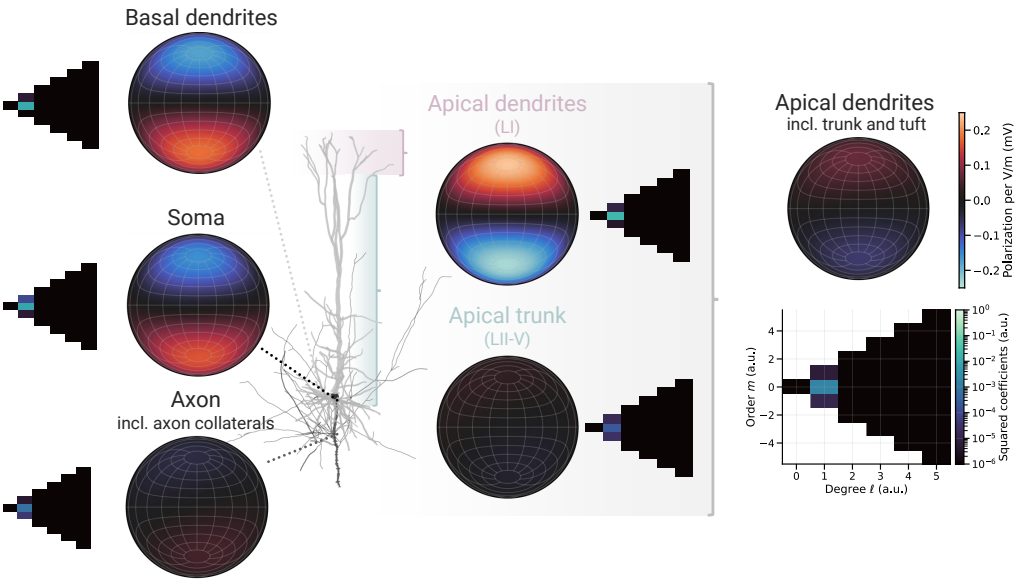

Figure 6. Models of different sections of a cell. Average response functions of different cell parts of a layer V (LV) early-branching thick-tufted pyramidal cell model and their 2D spectrums. In the morphology, the different cell parts considered are shown in different shades of gray. Models of apical dendrites are split in compartments belonging to L1, to the rest of layers and to the whole of the apical arborization. Coefficients are reported in table C1.

Cortical layer	Cell Morphology type	Membrane polarization δV (mV)	Displaced current δI_m (pA)	Ratio δV	Ratio δI_m
LII/III	Pyramidal	0.036	0.026	0.259	0.111
LIV	Pyramidal	0.052	0.027	0.377	0.114
LIV	Star pyramidal	0.019	0.005	0.141	0.022
LIV	Spiny stellate	0.025	0.014	0.185	0.060
LV	Untufted pyramidal	0.049	0.028	0.353	0.118
LV	Thick-tufted pyramidal (late)	0.089	0.122	0.645	0.524
LV	**Thick-tufted pyramidal (early)**	**0.138**	**0.233**	**1.000**	**1.000**
LV	Slender-tufted pyramidal	0.056	0.065	0.409	0.279
LVI	Untufted pyramidal	0.068	0.021	0.495	0.091
LVI	Tufted pyramidal (LI)	0.096	0.036	0.700	0.156
LVI	Tufted pyramidal (LIV)	0.119	0.030	0.867	0.129
LVI	Inverted pyramidal	0.104	0.027	0.756	0.114
LVI	Bipolar pyramidal	0.025	0.009	0.183	0.040

Table 1. Maximum observed somatic polarizations and transmamebrane currents and their respective ratio referenced to the largest. The cell type with the largest effect is the LV thick-tufted cell with an early branching of the apical tuft (bold).

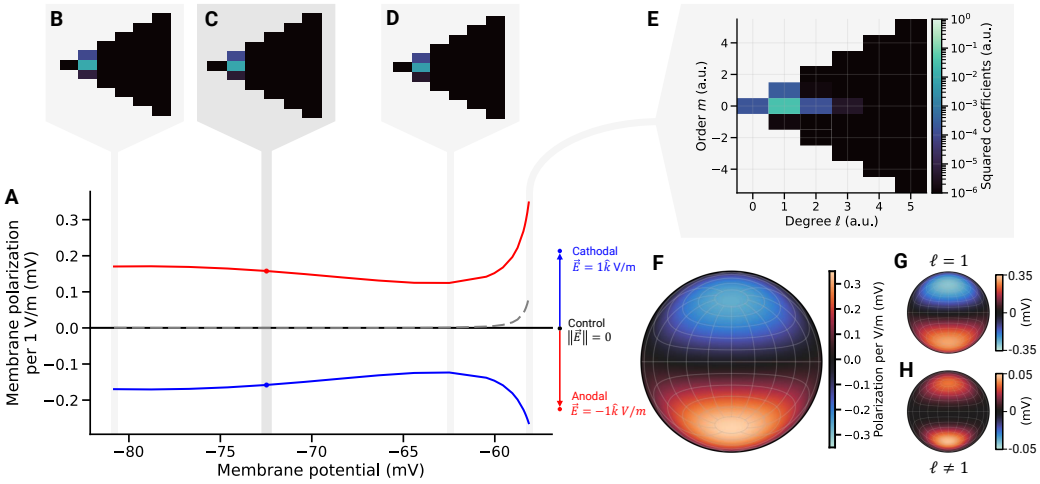

Figure 7. State dependence of somatic response to the electric field. **A.** Solid lines display the membrane polarization induced by an electric field of 1 V/m in anodal (red) and cathodal (blue) conditions. The control condition, i.e., zero-field, is displayed in black. The asymmetry between anodal and cathodal responses is displayed as the sum of both polarizations (dashed). The 2D spectrum of the response function is shown for hyperpolarization (**B**), resting (**C**), a depolarized state (**D**) and at the edge of the bifurcation (**E**). **F.** The response function at the edge of the bifurcation associated with E and its decomposition into dipolar (**G**, $\ell = 1$) and non-dipolar terms (**H**, $\ell \neq 1$).

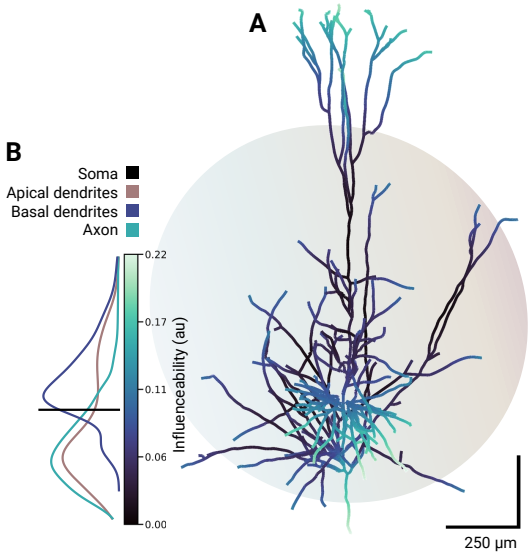

Figure 8. Influenceability values of a pyramidal cell. A. Variation of the influenceability measure throughout the morphology of an early-branching LV thick-tufted pyramidal cell. Scale: 250 µm. **B.** Distributions across compartments associated with different cell parts. The distribution of the apical dendrites displays bimodality, distinguishing the difference in values along the apical trunk from the values observed in the apical tuft.

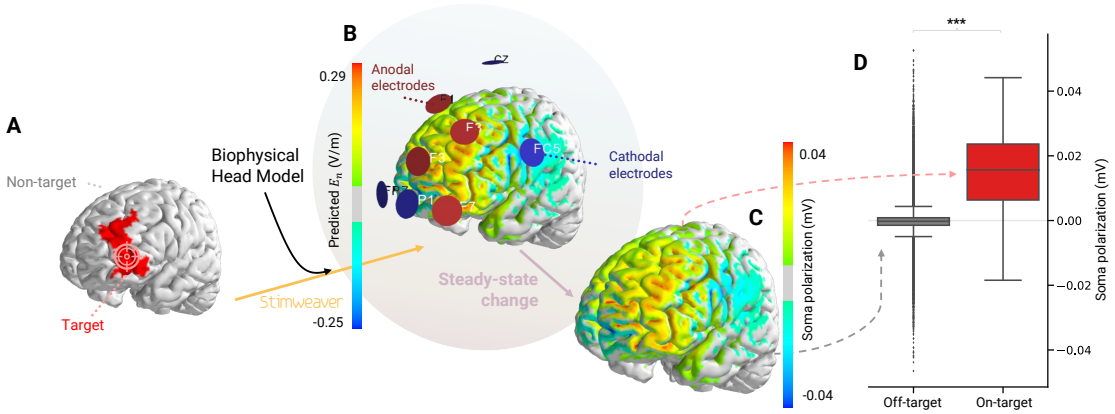

Figure 9. Predicted effects in a realistic montage Representation of a pipeline from a target definition to a predicted physiological effect. **A: Target definition.** Overlay in red of the cortical area marked as the target of the stimulation. In gray, the rest of the cortex. **B: Optimized montage.** Anodal (blue) and cathodal (red) electrodes location over the cortical surface. The predicted electric field magnitude is displayed color coded over the cortical surface, being the color code the one displayed in the colorbar on the left (V/m). **C: Predicted polarization.** Prediction of the somatic polarization of LV thick-tufted pyramidal cells. **D: Quantification of effects on and off target.** Predicted values of steady-state somatic polarization induced in a LV thick-tufted pyramidal cell using the optimized montage shown in B. The figure shows how effects are induced in the cortex selectively to the original target.

4. Discussion

One of the major goals of this study is the development of a simple and intuitive framework that allows the quantification of the effects of weak fields that can be used to build larger scale models. The values shown here for the juvenile rat reconstructions serve as a proof of concept that can be extrapolated to cell models of other species, or even adapting the same ones to match dimensions and other physiology features to that of adult rats or humans [13]. In fact, the approach is applicable to any multi-compartment model with a precise enough spatial resolution in its morphology.

Modeled effects from a dynamical systems perspective Equation 2 quantifies the displacement of the stable equilibrium of a neuron model under a weak electric field. As previously discussed, this requires that the model has this type of solution in the regime analyzed. However, neurons are excitable because they operate close to bifurcations that change the dynamical landscape, generally to give rise to periodic solutions, e.g., sustained firing. For instance, integrator models have a stable node (resting) and a saddle node. Short excitatory inputs push the system closer to the saddle node from the stable node, and if the system is pushed over the stable manifold of the saddle (threshold) it elicits an action potential on its excursion back to the stable point. A constant electric field works by persistently displacing the stable solution, and that is what the framework proposed quantifies, the shift of the stable node. This shift, in the example of an integrator model can be towards (excitatory) or away from (inhibitory) the spiking threshold. However, if the system is in an oscillatory regime, our formalism enters a problem of definition and cannot be strictly used anymore. A formalism in similar lines should be developed to describe changes in oscillatory solutions.

The main term in the spherical harmonic expansion is the dipolar one, (1,0) The expansion in spherical harmonics of the angular dependence of the effect provides a general framework that contains in its different terms different elements of interest. Relevant for stimulation models based on head models, in which one cannot know the azimuthal orientation of a cell with respect to the electric field induced, it becomes convenient that the expansion already collects in the $m = 0$ terms the behaviour that does not depend on the azimuth. In fact, by definition the $m = 0$ terms alone describe the *average* behaviour across all azimuths. Another relevant feature is that the method quantifies by definition the dipolar part of the response in its $\ell = 1$ terms, which we find to be the only present for most cases, in agreement with theoretical arguments (Appendix 2). This suggests that after the quantification, the steady-state shift can be represented by means of a dot product as it has been proposed in the literature under the λ E model framework [32]. Furthermore, in realistic settings where azimuthal information of single neurons is not available and for cells near rest, the only relevant term is thus the (1,0). However, we have observed how dipoles are not the only type of response and we observe asymmetries among anodal and cathodal responses, while

keeping a neutral response to perpendicular fields, in cells closer to threshold. In this case, we see the emergence of a 0-degree and 2-degree terms that correct the 1-degree ones by shifting the values at the poles of the dipole. For dipoles aligned with the z-axis (1,0), the emerging terms are a pair of equal value of (0,0) and (2,0). Equivalent expressions involving other terms can be found to modify dipoles oriented in other directions.

State-dependence In the neighborhood of the resting condition we observed an increase in size of the effect if the currents are hyperpolarizing and a decrease if depolarizing, as seen in Figure 7.A . This effect aligns with what is expected from the literature and consistent with the membrane resistance changes. That is, the size of the polarization induced by the external electric field depends on the membrane resistance. If the resistance increases, the magnitude of the effect should increase too [33]. However, we observe a different type of effect appearing close to the bifurcation. The emergence of other terms together with the increased excitability towards the spiking threshold requires a different interpretation. We suggest the origin of the effects are of different nature. For instance, with a simple model we can see that local changes of ion channels distribution can generate asymmetries in the local response to external fields. The window of increased excitability right before the spike is as well consistent with the typical effect of tDCS affecting spike times.

Reduced compartment models The average response of a cell part composed of different compartments can be obtained through averaging the coefficients of all the compartments. In other words, averaging the coefficients provides a model of the average response of selected segments or cell types. This strategy can be used to build an averaged response model of he axon, the apical dendrites, etc. This can be translated into multi-compartment models with just a few compartments that represent the local membrane dynamics of a few parts of a cell like the apical tuft, the soma or the axon initial segment, etc. Reducing the models here used to just a few compartments allow to use this knowledge in models at higher scales like models of cortical columns made of multi-compartmental cells. The ability to reduce cell models to just a few compartments reduces significantly the computation cost. At the limit, the effect of electric fields can also be represented in one compartment models as long as they are assumed to be modeling a specific part of the cell. This approach poses a proxy for stimulating commonly used models such as leaky or quadratic integrate and fire models [34].

Translation to mesoscale models, clinical relevance Computational models provide a powerful tool to understand the pathophysiology underlying neurological disorders such as epileptic activity. In [35] and more recently in [17], neural mass models (NMM) have been used to represent realistic epileptic seizure transitions: changes from interictal to ictal state were achieved by increasing the excitatory synaptic gain at the level of glutamatergic pyramidal cells and varying the inhibitory synaptic gains of GABAergic

interneurons. There is a growing interest in the use of non-invasive brain stimulation techniques as a potential treatment for drug-resistant patients, and, furthermore, in the use of computational models to optimize these treatments [36]. However, such models require the representation of the effects of electric fields on neuronal populations. The described methods are a starting point to derive the effects of weak, uniform electric fields at the population level (cortical column or small cortical patch scale). However, the translation from single cells to the mesoscale is not trivial given that there are network effects arising at the population level [14, 15]. A first approach can be to computationally obtain the response of a population by building models of cortical columns or networks of cell models and then extracting the effects at the population level. One could use a full cortical column model with multi-compartment models such as the one developed by the Blue Brain Project [25], and include the effect of the field at each compartment of each cell. A less computationally expensive approach could be to build a similar cortical column model made of neuron models with reduced numbers of compartments as introduced in the previous paragraph [37]. An alternative to assessing the population-scale effects computationally is to work in a theoretical framework that connects the microscale to the mesoscale starting from some simplifying assumptions. This kind of theoretical connection has recently grown in interest in the field of NMMs since the work by [21], who derived an exact mean field theory from the quadratic integrate and fire neuron model. In this framework, values for the induced transmembrane currents induced by weak fields as derived here are especially relevant, since there is no ambiguity in translating the effects from the microscale to the population level.

5. Conclusions

In this work we have provided a framework for analysis of the the effects of weak, uniform electric fields in neuron models in terms of changes in their steady-state conditions. We quantify the induced perturbation dependence on the orientation using spherical harmonic coefficients. Through this analysis, we have validated the commonly used dipole approximation for the studied models in their resting state and weak field regime. We have shown however that there are conditions under which this approximation is less accurate. Particularly, close to the spiking threshold. We have also seen that although pyramidal cells display in general the strongest effects, some interneurons are also affected but with a more diverse set of responses. Although the impact of these effects on networks of neurons is left for future research, this work provides the basis for further computational studies studying the relation of electric fields effects at microscale and mesoscales. This can benefit recent approaches involving brain modeling using neural mass model frameworks and derived clinical applications relying on brain stimulation with weak electric fields, such as tES.

Appendix A. Real spherical harmonics

A square-integrable function $f : S^2 \to \mathbb{R}$ can also be expanded in terms of the real harmonics $Y_{\ell m} : S^2 \to \mathbb{R}$, whose expression reads similarly:

$$f(\theta, \varphi) = \sum_{l=0}^{\infty} \sum_{m=-\ell}^{\ell} f_{\ell m} Y_{\ell m}(\theta, \varphi) \tag{A.1}$$

Where the real spherical harmonics are referred to as $Y_{\ell m}$.

Appendix A.1. Formal definition of the harmonics

The general definition of each spherical harmonic function $Y_{\ell m}$ can be cumbersome and its derivation is out of the scope of this text. For completeness, we summarize how they can be stated but it does not serve as an introduction to the field. Here it is worth-wile to recall the notation:

- θ stands for the polar angle or *inclination*.
- φ for the azimuth or *longitude*.
- ℓ for the spherical harmonic degree.
- m for the order.

Under this convention, the real spherical harmonics are defined as:

$$Y_{\ell m}(\theta, \varphi) = \begin{cases} \bar{P}_{\ell m}(\cos\theta) \cos m\varphi & \text{if } m \geq 0 \\ \bar{P}_{\ell |m|}(\cos\theta) \sin |m|\varphi & \text{if } m < 0 \end{cases}$$

where $\bar{P}_{\ell m}(\mu)$ are the normalized associated Legendre functions. For 4π-normalized spherical harmonic functions, they can be written as:

$$\bar{P}_{\ell m}(\mu) = \sqrt{(2 - \delta_{m0})\,(2\ell + 1)\frac{(\ell - m)!}{(\ell + m)!}} P_{\ell m}(\mu)$$

Note that δ_{ij} refers to the Kronecker delta and $P_{\ell m}(\mu)$ refers to the unnormalized associated Legendre functions. They can be derived from the standard Legendre polynomials using the relations shown below:

$$P_{\ell m}(\mu) = \left(1 - \mu^2\right)^{m/2} \frac{d^m}{d\mu^m} P_\ell(\mu)$$

$$P_\ell(\mu) = \frac{1}{2^l \ell!} \frac{d^\ell}{d\mu^\ell} \left(\mu^2 - 1\right)^\ell$$

As a set of basis functions, they need to be orthogonal. Note that the associated Legendre functions are indeed orthogonal for any given m, given that:

$$\int_{-1}^{1} \bar{P}_{\ell m}(\mu) P_{\ell m}(\mu) = 2\,(2 - \delta_{0m})\,\delta_{\ell\ell}$$

Appendix B. Dipole nature of electric field effect in compartment model of a neuron in the passive, linear membrane regime

Here we show that in the ohmnic, linear regime (far from threshold) or when the electric field is weak, the effect of an electric field on a neuron compartment, or its average over a set of compartments (uniform field), can be written in the form $\delta V = \mathbf{P} \cdot \mathbf{E}$, where $\mathbf{P}$ is a vector. This is the so-called "λE" model used in transcranial electrical stimulation models [32, 38].

The effect of an external field can be represented in a neuron compartment model by an axial current that results from the potential difference induced by the field along the fiber associated with a compartment

$$I = g^a \int_x^{x+\Delta x} E_x(s)\, ds \tag{B.1}$$

where E_x is the field along the fiber. We can rewrite this as $I = g^a \int_f \mathbf{E} \cdot d\mathbf{l}$ with the line integral along the fiber compartment. If the field is constant along the fiber we can express this simply as $I = \mathbf{E} \cdot \mathbf{u}$. The vector $\mathbf{u}$ is a vector parallel to the line that ends in the compartment of interest and originates in the connected one(s), and thus pointing into the compartment (see Figure B1). If the E field is aligned with this direction, we get a positive current into the compartment. If the compartment of interest is k and the connected compartment is j, we refer to the vector $\mathbf{u}_{k,j}$ parallel to $\mathbf{x}_k - \mathbf{x}_j$ (the coordinates of the compartments). The superscripts r and a refer to radial and axial components and conductivities.

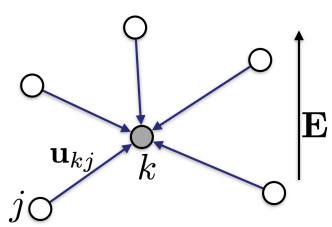

Figure B1. Compartments and vectors for cable equation in E field. Here we represent a fiber by a node and and a set of directed edges.

From conservation of charge (the sum over j is over connected compartments, and i over membrane currents), and assuming that the field is uniform and thus independent of the compartment k, we obtain

$$C_k \frac{dV_k}{dt} + \sum_i I_{i,k} = \sum_{j \leftrightsquigarrow k} g_j^a \left(V_j - V_k\right) + \sum_{j \leftrightsquigarrow k} g_j^a\, \mathbf{E} \cdot \mathbf{u}_{k,j} \tag{B.2}$$

The sum $\sum_{j \leftrightsquigarrow k} Q_j \equiv \sum_j c_{kj} Q_j$ denotes the sum over compartments connected to the kth one, and can be expressed via the compartment connectivity matrix c_{kj}, with value

of 1 if compartment j is connected to k, zero otherwise. The sum on the left hand side is over ionic membrane currents out of the compartment.

We can simplify this and also pull the constant electric field out the sum,

$$C_k \frac{dV_k}{dt} + I_k = \sum_{j \leftrightsquigarrow k} g_k^a (V_j - V_k) + \mathbf{p}_k \cdot \mathbf{E} \tag{B.3}$$

where $I_k = \sum_i I_{i,k}$, the k sum is over connected components to the kth compartment and where

$$\mathbf{p}_k = \sum_{j \leftrightsquigarrow k} g_j^a \mathbf{u}_{k,j} = \sum_j c_{kj} g_k^a \mathbf{u}_{k,j} \tag{B.4}$$

The equation for a single compartment in steady state is thus of the form

$$C_k \frac{dV_k}{dt} - \mathbf{p}_k \cdot \mathbf{E} + g_k^r V_k + I_k^0 + \sum_{j \leftrightsquigarrow k} g_j^a (V_k - V_j) = 0 \tag{B.5}$$

where $\mathbf{p}_k$ is the dipole vector corresponding to the kth compartment, and $I_k = V_k g_k^r + I_k^0$, with I^0 the sum of currents associated to the reversal potentials, and g_k^r the axial (transmembrane) conductivity in the linear regime.

Thus, we see that the behavior of each compartment is characterized by its own dipole and the interaction with other compartments.

Equation B.5 is linear and can be expressed in matrix form, with the compartment array notation $V = (V_k) = (V_1, V_2, \ldots, V_N)$, $C = \mathrm{diag}(C_k) = \mathrm{diag}(C_1, C_2, \ldots, C_N)$, and $(\mathbf{p}_k \cdot \mathbf{E}) = (\mathbf{p}_1 \cdot \mathbf{E}, \ldots, \mathbf{p}_N \cdot \mathbf{E})$,

$$C \frac{\partial V}{\partial t} + AV = I^0 - (\mathbf{p}_k \cdot \mathbf{E}) \tag{B.6}$$

and with the matrix A given by

$$A_{kj} = \delta_{kj} g_j^r - g_j^a c_{k,j} + \delta_{kj} \sum_l g_l^a c_{l,j} \tag{B.7}$$

In steady state ($\dot{V} = 0$), the solution to this equation is

$$V = A^{-1}[I^0 - (\mathbf{p}_k \cdot \mathbf{E})] \tag{B.8}$$

or

$$V_k = \sum_j A_{kj}^{-1} [I_k^0 - \mathbf{p}_k \cdot \mathbf{E}] = \sum_j A_{kj}^{-1} - \mathbf{E} \cdot \sum_j A_{kj}^{-1} \mathbf{p}_j \tag{B.9}$$

where the second equality is a result of linearity of the A matrix, i.e., the fact that we are dealing with a linear equation. Finally, we can write the solution as

$$V_k = \sum_j A_{kj}^{-1} I_j^0 + P_k \cdot E \tag{B.10}$$

This equation shows that the response of the compartment to an electric field is of dipole form, with the total dipole P_k resulting from a superposition of dipoles,

$$\mathbf{P}_k = -\sum_j A^{-1}_{kj}\mathbf{p}_j = -\sum_{j,l} A^{-1}_{kj}\, c_{jl} g^a_j \mathbf{u}_{j,l} \tag{B.11}$$

Furthermore, we observe that any linear function of compartment potentials will also display, by further superposition, a dipole response. This includes, for example, the average membrane perturbation for apical dentrite compartments, or soma.

What happens in the **nonlinear case**, when the neuron is not at baseline? We can write (steady state)

$$-p_k \cdot \mathbf{E} + I^r_k(V_k) + \sum_{j \rightsquigarrow k} g^a_j (V_k - V_j) = 0 \tag{B.12}$$

with $I^r_k(V_k)$ a nonlinear function, or, in a fashion analogous to the discussion above, in matrix form

$$-p_k \cdot \mathbf{E} + BV + I(V) = 0$$

or

$$F_k(V) = \mathbf{p}_k \cdot \mathbf{E} \tag{B.13}$$

for a nonlinear operator F. This means we cannot pull out the E field out of the inverse. However, if the electric field is very weak, we can carry out the analysis above with the linearized version of Equation B.13 by expanding it around the potential with zero field, with the same conclusion.

Appendix C. Supplementary tables and figures

Table C1. Spherical harmonic coefficients of the response observed in different cell parts of a layer V thick-tufted pyramidal reconstructed cell model.

	Apical	Axon	Basal	Soma
(0, 0)	0.000269004	-0.000260209	-7.28E-05	-8.07E-05
(1, -1)	-0.003474872	0.006142342	-0.000209493	0.002328097
(1, 0)	0.041506581	-0.025128212	-0.103012672	-0.090822117
(1, 1)	-0.002554922	0.002155694	0.002506737	-0.010029683
(2, -2)	8.11E-07	-1.26E-05	-2.85E-07	-2.22E-07
(2, -1)	6.38E-07	2.56E-06	-2.28E-06	-2.88E-06
(2, 0)	0.000201417	-0.000156987	-8.87E-05	-9.50E-05
(2, 1)	8.95E-06	8.25E-06	-6.00E-06	-5.83E-06
(2, 2)	-9.89E-06	1.65E-05	-5.27E-06	-5.19E-06
(3, -3)	-6.71E-09	-6.81E-09	-5.59E-09	-5.32E-09
(3, -2)	-6.96E-09	-7.92E-09	-1.56E-08	-1.54E-08
(3, -1)	1.56E-08	6.54E-08	4.13E-08	3.78E-08
(3, 0)	7.77E-07	-1.84E-08	5.53E-07	5.50E-07
(3, 1)	8.62E-08	3.90E-08	4.62E-08	4.91E-08
(3, 2)	-3.19E-08	-4.24E-09	-3.13E-08	-3.02E-08
(3, 3)	-3.07E-09	-4.22E-09	-3.02E-09	-2.75E-09
(4, -4)	-9.39E-12	-4.23E-11	-3.46E-13	-4.16E-13
(4, -3)	-8.21E-11	-3.38E-11	-4.45E-11	-4.37E-11
(4, -2)	-1.71E-10	-8.52E-11	-9.84E-11	-9.90E-11
(4, -1)	1.71E-10	5.51E-10	6.73E-10	6.73E-10
(4, 0)	5.44E-10	3.64E-09	5.16E-09	5.28E-09
(4, 1)	1.19E-10	1.48E-10	1.82E-10	1.93E-10
(4, 2)	2.91E-10	4.35E-11	-1.95E-11	-1.11E-11
(4, 3)	6.25E-11	1.46E-11	2.51E-13	2.41E-12
(4, 4)	3.27E-13	-6.69E-12	4.28E-12	3.95E-12
(5, -5)	9.75E-15	4.67E-14	1.11E-14	1.19E-14
(5, -4)	-2.80E-15	-5.73E-14	-1.85E-14	-1.80E-14
(5, -3)	-3.45E-13	-3.11E-13	-1.60E-13	-1.62E-13
(5, -2)	-1.51E-12	-5.01E-14	-2.66E-13	-2.80E-13
(5, -1)	-1.76E-12	-1.18E-12	-1.26E-12	-1.28E-12
(5, 0)	-4.01E-11	2.43E-12	-1.90E-11	-1.92E-11
(5, 1)	-4.20E-12	-8.62E-14	-1.30E-12	-1.33E-12
(5, 2)	5.01E-12	1.03E-12	1.57E-12	1.63E-12
(5, 3)	7.95E-13	-7.65E-14	1.57E-13	1.69E-13
(5, 4)	-4.13E-14	-1.27E-14	-5.17E-15	-6.70E-15
(5, 5)	-1.08E-14	-6.81E-14	-6.35E-15	-5.73E-15

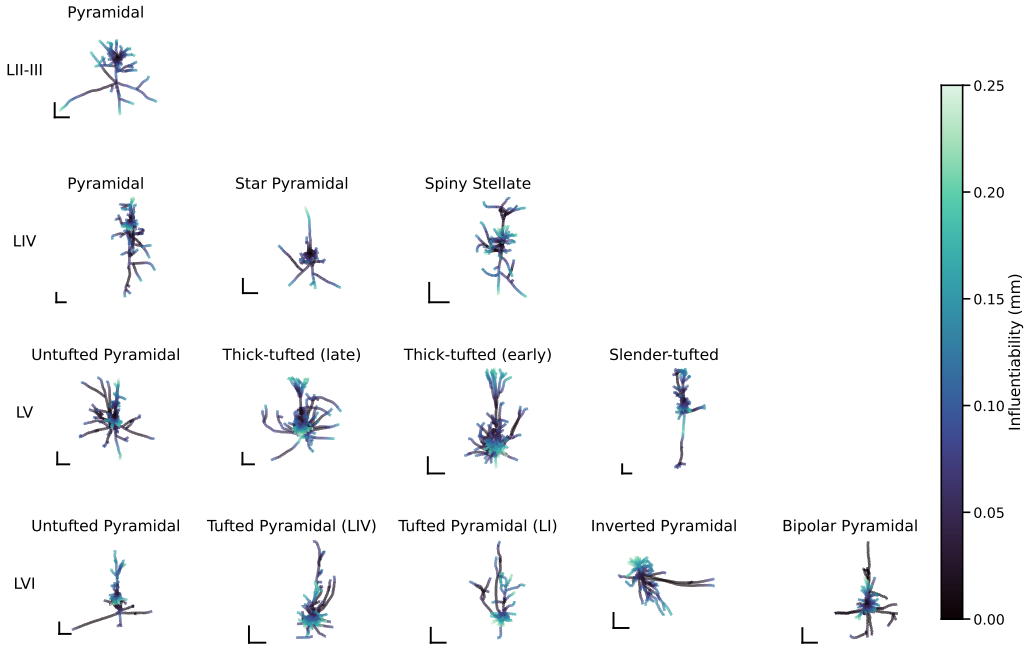

Figure C1. Pyramidal cells influentiabilities. Variation of the influentiability measure throughout the morphology of different pyramidal cell types. The representative of each cell type is chosen as the neuron with the highest influentiablity value in the soma. Spatial scale is maintained and all cells are aligned horizontally through the soma. Scale: 250 µm.

Acknowledgments

This work has received funding from the European Research Council (ERC) under the European Union's Horizon 2020 research and innovation programme (grant agreement No 855109; ERC-SyG 2019) and from FET under the European Union's Horizon 2020 research and innovation programme (grant agreement No 101017716).

References

[1] M. A. Nitsche and W. Paulus. Excitability changes induced in the human motor cortex by weak transcranial direct current stimulation. *J Physiol*, 527 Pt 3:633–9, 2000.

[2] D. Liebetanz, F. Fregni, K. K. Monte-Silva, M. B. Oliveira, A. Amancio-dos Santos, M. A. Nitsche, and R. C. Guedes. After-effects of transcranial direct current stimulation (tDCS) on cortical spreading depression. *Neurosci Lett*, 398(1-2):85–90, 2006.

[3] D. Liebetanz, M. A. Nitsche, F. Tergau, and W. Paulus. Pharmacological approach to the mechanisms of transcranial DC-stimulation-induced after-effects of human motor cortex excitability. *Brain*, 125(2238-2247), 2002.

[4] Giulio Ruffini, Fabrice Wendling, Isabelle Merlet, Behnam Molaee-Ardekani, Abeye Mekonnen, Ricardo Salvador, Aureli Soria-Frisch, Carles Grau, Stephen Dunne, and Pedro C. Miranda. Transcranial current brain stimulation (tCS): Models and technologies. *IEEE Transactions on Neural Systems and Rehabilitation Engineering*, 21(3):333–345, May 2013.

[5] Pedro Cavaleiro Miranda, Abeye Mekonnen, Ricardo Salvador, and Giulio Ruffini. The electric field in the cortex during transcranial current stimulation. *Neuroimage*, 70:45–58, 2013.

[6] P. C. Miranda, M. Hallett, and P. J. Basser. The electric field induced in the brain by magnetic stimulation: a 3-D finite-element analysis of the effect of tissue heterogeneity and anisotropy. *IEEE Trans Biomed Eng*, 50(9):1074–85, 2003.

[7] Frank Rattay. Analysis of models for external stimulation of axons. *IEEE Transactions on Biomedical Engineering*, 33(10):974–977, 1986.

[8] Thomas Radman, Raddy L. Ramos, Joshua C. Brumberg, and Marom Bikson. Role of cortical cell type and morphology in subthreshold and suprathreshold uniform electric field stimulation in vitro. *Brain Stimulation*, 2(215):28, 2009.

[9] W. Rall. Core conductor theory and cable properties of neurons. pages 39–97. American Physiological Society, 1977.

[10] D. Tranchina and C. Nicholson. A model for the polarization of neurons by extrinsically applied electric fields. *Biophys J*, 50(6):1139–56, 1986.

[11] Frank Rattay. Analysis of models for extracellular fiber stimulation. *IEEE Transactions on Biomedical Engineering*, 36(7):676–682, 1989.

[12] B. J. Roth. Mechanisms for electrical stimulation of excitable tissue. *Crit Rev Biomed Eng*, 22(3-4):253–305, 1994.

[13] Aman S Aberra, Angel V Peterchev, and Warren M Grill. Biophysically realistic neuron models for simulation of cortical stimulation. *Journal of Neural Engineering*, 15(6):066023, October 2018.

[14] F Fröhlich and D. A. McCormick. Endogenous Electric Fields May Guide Neocortical Network Activity. *Neuron*, 67:129–143, 2010.

[15] D. Reato, A. Rahman, M. Bikson, and L. C. Parra. Low-intensity electrical stimulation affects network dynamics by modulating population rate and spike timing. *Journal of Neuroscience*, 30(45):15067–15079, November 2010.

[16] Giulio Ruffini, Ricardo Salvador, Ehsan Tadayon, Roser Sanchez-Todo, Alvaro Pascual-Leone, and Emiliano Santarnecchi. Realistic modeling of mesoscopic ephaptic coupling in the human brain. *PLoS Comput. Biol.*, 2020.

[17] E. Lopez-Sola and et al. A realistic unified neural mass model of ictalactivity. *to be submitted*, 2021.

[18] B. H. Jansen, G. Zouridakis, and M. E. Brandt. A neurophysiologically-based mathematical model of flash visual evoked potentials. *Biol Cybern*, 68(3):275–83, 1993.

[19] B. H. Jansen and V. G. Rit. Electroencephalogram and visual evoked potential generation in a mathematical model of coupled cortical columns. *Biol Cybern*, 73(4):357–66, 1995.

[20] F. Grimbert and Olivier Faugeras. Analysis of Jansen's model of a single cortical column. *INRIA*, RR-5597:34, June 2006.

[21] Ernest Montbrió, Diego Pazó, and Alex Roxin. Macroscopic description for networks of spiking neurons. *Phys. Rev. X*, 021028, 2015.

[22] Federico Devalle, Alex Roxin, and Ernest Montbrió. Firing rate equations require a spike synchrony mechanism to correctly describe fast oscillations in inhibitory networks. *PLOS Computational Biology*, 13(12), 2017.

[23] Giulio Ruffini. Analysis and extension of exact mean-field theory with dynamic synaptic currents. *bioRxiv*, (https://www.biorxiv.org/content/10.1101/2021.09.01.458563v6), 2021.

[24] Giulio Ruffini, Michael D. Fox, Oscar Ripolles, Pedro Cavaleiro Miranda, and Alvaro Pascual-Leone. Optimization of multifocal transcranial current stimulation for weighted cortical pattern targeting from realistic modeling of electric fields. *NeuroImage*, 89:216 – 225, 2014.

[25] Henry Markram, Eilif Muller, Srikanth Ramaswamy, Michael W. Reimann, Marwan Abdellah, Carlos Aguado Sanchez, Anastasia Ailamaki, Lidia Alonso-Nanclares, Nicolas Antille, Selim Arsever, Guy Antoine Atenekeng Kahou, Thomas K. Berger, Ahmet Bilgili, Nenad Buncic, Athanassia Chalimourda, Giuseppe Chindemi, Jean-Denis Courcol, Fabien Delalondre, Vincent Delattre, Shaul Druckmann, Raphael Dumusc, James Dynes, Stefan Eilemann, Eyal Gal, Michael Emiel Gevaert, Jean-Pierre Ghobril, Albert Gidon, Joe W. Graham, Anirudh Gupta, Valentin Haenel, Etay Hay, Thomas Heinis, Juan B. Hernando, Michael Hines, Lida Kanari, Daniel Keller, John Kenyon, Georges Khazen, Yihwa Kim, James G. King, Zoltan Kisvarday, Pramod Kumbhar, Sébastien Lasserre, Jean-Vincent Le Bé, Bruno R.C. Magalhães, Angel Merchán-Pérez, Julie Meystre, Benjamin Roy Morrice, Jeffrey Muller, Alberto Muñoz-Céspedes, Shruti Muralidhar, Keerthan Muthurasa, Daniel Nachbaur, Taylor H. Newton, Max Nolte, Aleksandr Ovcharenko, Juan Palacios, Luis Pastor, Rodrigo Perin, Rajnish Ranjan, Imad Riachi, José-Rodrigo Rodríguez, Juan Luis Riquelme, Christian Rössert, Konstantinos Sfyrakis, Ying Shi, Julian C. Shillcock, Gilad Silberberg, Ricardo Silva, Farhan Tauheed, Martin Telefont, Maria Toledo-Rodriguez, Thomas Tränkler, Werner Van Geit, Jafet Villafranca Díaz, Richard Walker, Yun Wang, Stefano M. Zaninetta, Javier DeFelipe, Sean L. Hill, Idan Segev, and Felix Schürmann. Reconstruction and simulation of neocortical microcircuitry. *Cell*, 163(2):456–492, October 2015.

[26] Cameron C. McIntyre and Warren M. Grill. Extracellular stimulation of central neurons: Influence of stimulus waveform and frequency on neuronal output. *Journal of Neurophysiology*, 88(4):1592–1604, October 2002.

[27] Mark A. Wieczorek and Matthias Meschede. SHTools: Tools for working with spherical harmonics. *Geochemistry, Geophysics, Geosystems*, 19(8):2574–2592, August 2018.

[28] M. L. Hines and N. T. Carnevale. NEURON: a tool for neuroscientists. *Neuroscientist*, 7(2):123–35, 2001.

[29] Huan Wang, Bonnie Wang, Kieran P. Normoyle, Kevin Jackson, Kevin Spitler, Matthew F. Sharrock, Claire M. Miller, Catherine Best, Daniel Llano, and Rose Du. Brain temperature and its fundamental properties: a review for clinical neuroscientists. *Frontiers in Neuroscience*, 8, October 2014.

[30] J.R. Driscoll and D.M. Healy. Computing fourier transforms and convolutions on the 2-sphere. *Advances in Applied Mathematics*, 15(2):202–250, June 1994.

[31] M. Bikson, M. Inoue, H. Akiyama, J. K. Deans, J. E. Fox, H. Miyakawa, and J. G. Jefferys. Effects of uniform extracellular DC electric fields on excitability in rat hippocampal slices in vitro. *J*

Physiol, 557(Pt 1):175–90, 2004.

[32] Giulio Ruffini, Fabrice Wendling, Isabelle Merlet, Behnam Molaee-Ardekani, Abeye Mekkonen, Ricardo Salvador, Aureli Soria-Frisch, Carles Grau, Stephen Dunne, and Pedro Miranda. Transcranial Current Brain Stimulation (tCS): Models and Technologies. *IEEE Transactions on Neural Systems and Rehabilitation Engineering*, 21(3):333–345, May 2013.

[33] Walter Paulus and John C. Rothwell. Membrane resistance and shunting inhibition: where biophysics meets state-dependent human neurophysiology. *The Journal of Physiology*, 594(10):2719–2728, May 2016.

[34] Peter Dayan and L F Abbott. *Theoretical neuroscience*. Computational neuroscience. MIT Press, London, England, December 2001.

[35] F. Wendling, F. Bartolomei, J. J. Bellanger, and P. Chauvel. Epileptic fast activity can be explained by a model of impaired GABAergic dendritic inhibition. *Eur J Neurosci*, 15(9):1499–508, 2002.

[36] Giulio Ruffini, Fabrice Wendling, Roser Sanchez-Todo, and Emiliano Santarnecchi. Targeting brain networks with multichannel transcranial current stimulation (tCS). *Current Opinion in Biomedical Engineering*, 2018.

[37] Yves Denoyer, Isabelle Merlet, Fabrice Wendling, and Pascal Benquet. Modelling acute and lasting effects of tDCS on epileptic activity. *Journal of Computational Neuroscience*, 48(2):161–176, May 2020.

[38] Giulio Ruffini, Michael D Fox, Oscar Ripolles, Pedro Cavaleiro Miranda, and Alvaro Pascual-Leone. Optimization of multifocal transcranial current stimulation for weighted cortical pattern targeting from realistic modeling of electric fields. *Neuroimage*, 89:216–225, 2014.